Four-wave mixing in the diamond configuration in an atomic vapor

R. T. Willis,[1,*] F. E. Becerra,[2,1] L. A. Orozco,[1] and S. L. Rolston[1]
[1]*Joint Quantum Institute, Department of Physics, University of Maryland, Maryland 20742, USA and National Institute of Standards and Technology, College Park, Maryland 20742, USA*
[2]*Departamento de Física, CINVESTAV, Apdo. Post. 14-740, 07000 Mexico, Distrito Federal, Mexico*
(Received 29 December 2008; published 12 March 2009)

We present measurements of the resonance structure for nondegenerate four-wave mixing (4WM) in the diamond configuration in a warm atomic vapor of rubidium. We show that a narrow sub-Doppler feature exists and can be understood as a result of velocity-class selection. We measure the efficiency of the 4WM process and show it to be on the order of 1×10^{-4}. Our observations are consistent with the results of a theoretical treatment based on the semiclassical Maxwell-Bloch equations for the system with the appropriate coupling values derived from the experimental values in Rb.

DOI: 10.1103/PhysRevA.79.033814 PACS number(s): 42.65.Hw, 42.65.Ky, 42.50.Gy

I. INTRODUCTION

Four-wave mixing (4WM) in atomic vapors has been explored extensively in the past. Some of the original work investigated basic nonlinear optics, interference phenomena among various optical processes [1], and the generation of squeezed light [2]. Recent work in 4WM in atomic vapors has lead to large twin-beam multimode squeezing with possible applications to quantum imaging [3,4]. Other work has shown some of the tools necessary for long-distance quantum communication including optical qubit storage and retrieval [5,6].

Much of the recent literature has exploited the Λ or double-Λ atomic level structure, which benefits from coherence between the two lower stable states. Here we concern ourselves with a warm ensemble of atoms in the diamond configuration, illustrated in Fig. 1. The diamond level structure has one stable ground state, two intermediate levels, and one top state, pairwise coupled by the electromagnetic field as indicated. Earlier theoretical work has shown that this level structure gives rise to interesting phase-sensitive propagation behavior [7]. Also, polarization entangled photon pairs have been demonstrated via spontaneous 4WM from both a laser-cooled ensemble [8] and in a warm ensemble [9] like the one we consider here. The complicated resonance structure of a strongly driven diamond system has been investigated in Ref. [10]. Note that in rubidium the upper state can be chosen such that the frequencies of the light fields are at telecommunications wavelengths (1.3 μm for the 6S and 1.5 μm for the 4D), and may have possible applications for quantum communication [8]. With all of this in mind, it is the goal of this work to understand some of the basic aspects of the 4WM process in this system.

We investigate 4WM in a warm atomic vapor of Rb atoms. We are concerned with the basic resonance structure of the 4WM interaction in a thermal medium, as well as the efficiency of the process. In the following Sec. II we discuss the experiment and present our measurements. In Sec. III we describe a simple theoretical treatment based on the semiclassical Maxwell-Bloch equations that show agreement with our data. We conclude in section in Sec. IV with some of the calculations presented in the Appendix.

II. EXPERIMENT

We apply three lasers beams to a 1.5 cm long vapor cell of isotopically pure ^{85}Rb to investigate the resonance structure of the 4WM. The cell is heated to 100 °C with a resistive heater. The three applied laser beams intersect in the center of the cell at small angles. The beams are at 795 nm (ω_1), 1324 nm (ω_2), and 780 nm (ω_4), with wave vectors $\vec{k}_1$, $\vec{k}_2$, and $\vec{k}_4$, respectively (see Fig. 2). The beam waist of the applied laser fields are all approximately 1 mm. We work in a regime in which all the applied laser beams are above the saturation intensity. Both the 795 and 1324 nm beams are horizontally polarized. The polarization of the generated beam is then the same as the 780 nm laser polarization which we arbitrarily chose to be vertical. The efficiency of the process does not depend strongly on the choice of 780 nm pump polarization. The generated beam with angular frequency ω_3 and wave vector $\vec{k}_3$ must fulfill energy conservation and the phase matching condition, namely,

$$\omega_1+\omega_2=\omega_3+\omega_4, \tag{1}$$

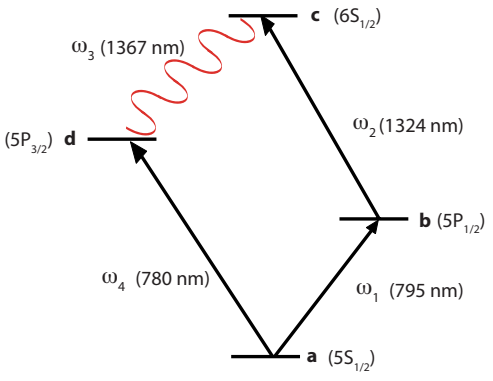

FIG. 1. (Color online) The diamond level structure in rubidium. In the experiment we apply fields 1, 2, and 4, and measure the generated light denoted by field 3.

*tommyw@physics.umd.edu

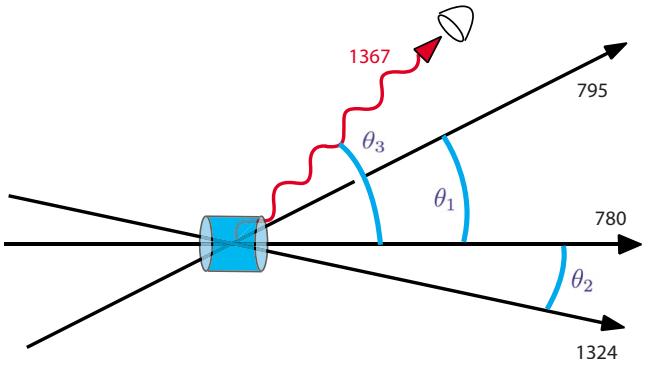

FIG. 2. (Color online) Schematic diagram of the experimental set up. The incident and generated beams are at the angles $\theta_1=2°$, $\theta_2=0.7°$, and $\theta_3=2.7°$. The 1367 nm generated light (red) is collected with a InGaAs photodiode.

$$\vec{k}_1+\vec{k}_2=\vec{k}_3+\vec{k}_4. \tag{2}$$

Although we will not use it in the discussion here, we should point out that there exists a third conservation law related to angular momentum that creates particular correlations among the photons and the magnetic sublevels of the process (see Ref. [8]).

A. Resonance structure

First, we observe the intensity of the generated light at 1367 nm as a function of the detuning of the 1324 and 780 nm lasers. The 795 nm laser is locked 1.5 GHz red-detuned from the D_1 line using RF sidebands and saturated absorption on an auxiliary Rb cell. We scan the 1324 nm laser across the two-photon resonance and the 780 nm laser across the D_2 Doppler peak. In Fig. 3 we plot the intensity of the generated 1367 nm light which exhibits a narrow Gaussian-like resonance.

Figure 4 shows a slice of the surface plotted in Fig. 3 at a constant 1324 detuning. We lock the 795 nm laser 1.5 GHz red of the D_1 line while the 1324 nm laser is locked such that the two lasers together are resonant with the $(5S_{1/2},\ F=3) \rightarrow (6S_{1/2},\ F=3)$ two-photon resonance. The 1324 nm laser is locked using a digital transfer-cavity lock [11]. We scan the 780 nm laser over the D_2 line. There are three peaks in the 4WM signal corresponding to the three allowed intermediate hyperfine states. The largest peak involves the $F=4$ intermediate state.

B. Generation efficiency

It is important to consider the efficiency of conversion from 780 nm photons to 1367 nm photons for application in various quantum communication protocols. Figure 5 shows the power in the generated light as a function of the power in the 780 beam for several different 795 laser powers. The efficiency is never greater than 1×10^{-4}, due to the absorption of the medium (see Sec. III). The residual magnetic field (<1 G) does not affect the efficiency in any significant way.

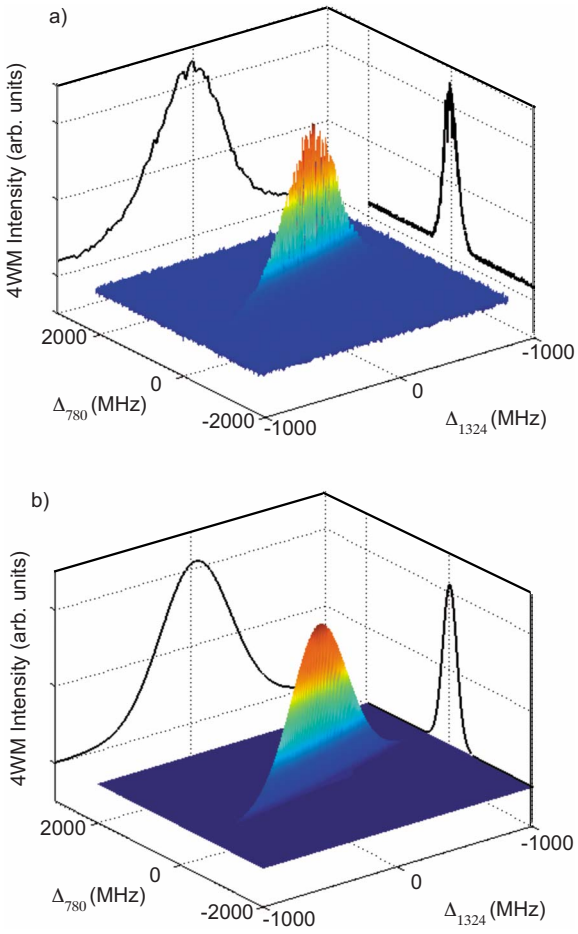

FIG. 3. (Color online) Generated 1367 nm intensity as a function of 780 and 1324 detuning. The narrow feature is a result of velocity-class selection. For this example $P_{780}=3$ mW, $P_{795}=100$ mW, and $P_{1324}=5$ mW. The 795 nm laser was detuned 1.5 GHz red of the D_1 $F=3\rightarrow F=2,3$ peak. The data appears in a), b) is our model (discussed below).

III. THEORY AND ANALYSIS

We are concerned in this section with understanding the origin of the sharp peak in Fig. 3(a) and the efficiency of the 4WM process. To this end we apply the density-matrix formalism and solve the Maxwell-Bloch (MB) equations [12].

A. Maxwell-Bloch treatment

We model the system with the standard density-matrix treatment including spontaneous decay. We have a four-level atom with the structure indicated in Fig. 1. Our atoms are coupled to an electromagnetic field of the form

$$E(z,t)=\sum_{i=1}^{4}[E_i(z)e^{i(k_iz-\omega t)}+\text{c.c.}]. \tag{3}$$

We use the notation indicated in Fig. 1 in which the generated beam is of frequency $\omega_3=\omega_1+\omega_2-\omega_4$. The propagation direction of each laser is given by $\vec{k}_i$, where $|\vec{k}_i|=2\pi/\lambda_i$. We define the one-photon detunings as $\Delta_{ba}=\omega_{ba}-\omega_1$, $\Delta_{cb}=\omega_{cb}-\omega_2$, $\Delta_{cd}=\omega_{cd}-\omega_3$, and $\Delta_{ba}=\omega_{ba}-\omega_4$. The two-photon de-

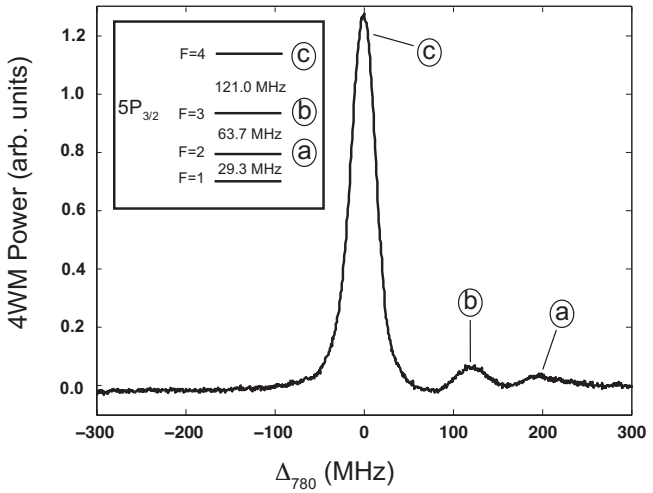

FIG. 4. The intensity of the generated 1367 nm beam as a function of 780 nm detuning. The inset shows the $5P_{3/2}$ hyperfine structure which is the origin of the three observed peaks.

tunings are $\Delta_{ca}=\Delta_{cb}+\Delta_{ba}$ and $\Delta_{bd}=\Delta_{ba}-\Delta_{da}$. We define γ_{ij} to be the atomic decay rate in radians per second from level i to j and Γ_{ij} to be the average of the total decay rates from levels i and j. Finally, we define the spatially varying Rabi frequencies $\Lambda_{ba}=E_1(z)e^{i\vec{k}_1 z}\mu_{ba}/\hbar$, $\Lambda_{cb}=E_2(z)e^{i\vec{k}_2 z}\mu_{cb}/\hbar$, $\Lambda_{cd}=E_3(z)e^{i\vec{k}_3 z}\mu_{cd}/\hbar$, and $\Lambda_{da}=E_4(z)e^{i\vec{k}_4 z}\mu_{da}/\hbar$. We also factor out the fast time dependence of the laser fields from the density matrix elements such that $\rho_{ij}=\sigma_{ij}\exp(-i\omega_{ij}t)$. With these definitions the density-matrix equations become

$$\dot{\sigma}_{ll}=\sum_j \gamma_{jl}\sigma_{jj}-\sum_j \gamma_{lj}\sigma_{ll}+i\sum_j (\Lambda_{lj}\sigma_{jl}-\Lambda_{jl}\sigma_{lj}),$$

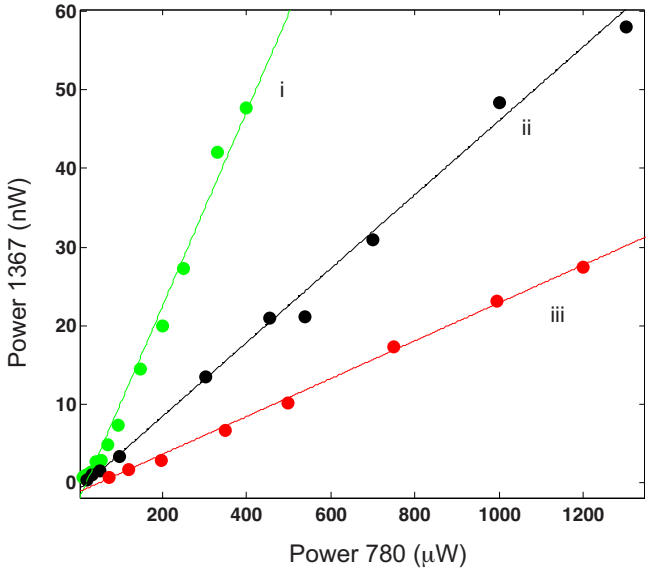

FIG. 5. (Color online) The power in the generated 1367 nm beam for different 780 powers. Each line is for a different 795 power: (i) $P_{795}=115$ mW, (ii) $P_{795}=50$ mW, and (iii) $P_{795}=15$ mW. The power in the 1324 nm laser is 5 mW and efficiency is between 1×10^{-4} to 1×10^{-5} in all cases.

$$\dot{\sigma}_{nl}=-(i\Delta_{nl}+\Gamma_{nl})\sigma_{nl}+i\sum_j (\Lambda_{nj}\sigma_{jl}-\Lambda_{jl}\sigma_{nj}). \quad (4)$$

We can write these equations in the form $R\vec{\sigma}=\dot{\vec{\sigma}}$ where R is a 16×16 matrix and $\vec{\sigma}$ is a length-16 vector containing the elements of the density matrix. In the steady state this reduces to $R\vec{\sigma}_s=\vec{0}$. Because of conservation of population the rows R are not independent and therefore we replace the σ_{aa} equation with the trace condition, $\Sigma_i\rho_{ii}=1$. Then the equation to solve is $R\vec{\sigma}_s=\vec{y}$, where $\vec{y}=(1\ 0\ 0\ 0\ \ldots)^T$.

Note that since we are discussing a thermal ensemble of atoms, the motion of the atoms will be an important factor in the emission spectrum. Atomic motion can be included through the Doppler shift of the various laser detunings for each velocity v, e.g., $\Delta_{ba}^v=\omega_{ba}-\omega_1+\vec{k}_1\cdot\vec{v}$. Integrating each density-matrix element over the Boltzmann distribution then gives

$$\bar{\sigma}_{ij}=\int \rho(v)\sigma_{ij}(v)dv, \quad (5)$$

where $\rho(v)=\sqrt{m/(2\pi k_b T)}\exp[-mv^2/(2k_b T)]$.

In some cases it is sufficient to calculate the steady-state polarization of the medium. In others, particularly when several competing processes are at work, such as 4WM and absorption, one must take propagation into account. For an electromagnetic field propagating in an atomic medium with a polarization of the form

$$P(z,t)=\sum_{i=1}^{4}[P_i(z)e^{-i\omega_i t}+\text{c.c.}], \quad (6)$$

the wave equation in the slowly varying amplitude approximation becomes

$$\partial_z E_i=2\pi|k|ie^{-ik_i z}P_i(z). \quad (7)$$

The atomic polarization is related to the density matrix through $P=N\langle\mu\rangle=N\,\mathrm{Tr}(\rho\mu)$. The polarization of the medium that contributes as a source for the 4WM process is $P_3(z)=N\mu_{dc}\bar{\sigma}_{cd}$, with similar expressions for the other P_i. We solve the coupled set of equations for the field and atoms down the length of the atomic ensemble. We neglect any possible transverse effects.

Figure 6 shows a typical solution to the MB equations with $\Delta_{ba}=-\Delta_{cb}=1500$ MHz$\times2\pi$. The incident intensities are $I_1=I_2=10$ mW/cm^2 and $I_4=1$ mW/cm^2. Figure 6(a) shows the intensity of fields 3 and 4 as a function of propagation distance in the medium. Linear absorption dominates the behavior of field 4 while parametric 4WM leads to the generation of field 3. In Fig. 3(b) we see the polarization of the generated beam, P_3, as a function of propagation distance and velocity of the atoms in the medium. The polarization decreases as a function of length due to the absorption of the field 4 while only a narrow band of velocities, centered around $v=0$ for the parameters used here, contributes to the 4WM process.

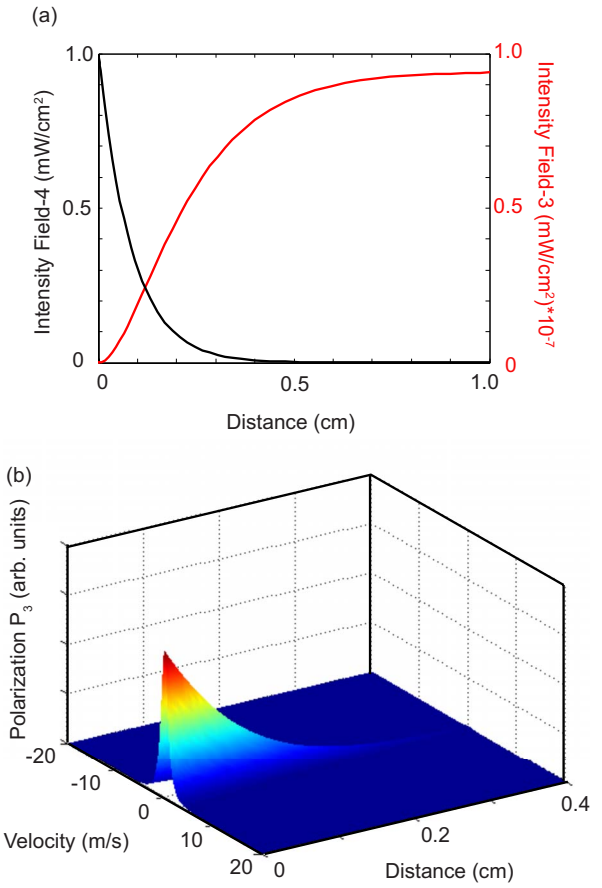

FIG. 6. (Color online) Typical solution to the MB equations in the diamond system. (a) The intensity of fields 3 and 4 as a function of propagation distance. (b) The polarization, P_3, of the generated field as a function of propagation distance and velocity class.

B. Velocity selective 4WM

Figure 3(b) shows a plot of $|\sigma_{cd}|^2$ solved numerically for parameters close to that of the experiment. For large detuning of the 795 nm field the data and model show a narrow sub-Doppler feature, in clear qualitative agreement.

Intuitively this feature can be explained by the fact that the 4WM process is strongest in resonant atoms. Since we are working in a thermal cell, given a set of proper detunings, only one velocity class (a group of atoms all moving with roughly the same velocity with spread $\sigma_v \approx \gamma/k$, where k and γ are some characteristic wave vector and atomic linewidth, respectively) will be resonant for 4WM at a time. To lowest nonzero order the solution to Eq. (4) for the polarization component which contributes to simple 4WM is proportional to

$$\sigma_{cd}^{\mathrm{PM}} = \frac{\Lambda_{ad}\Lambda_{ba}\Lambda_{cd}}{(\Delta_{ba} - i\Gamma_{ba})(\Delta_{da} + i\Gamma_{da})(\Delta_{ca} - i\Gamma_{ca})}, \tag{8}$$

where PM stands for phase matched. In the present case the 795 nm (ω_1) laser is so far off resonance ($\Delta_{ba} \approx 1.5$ GHz) that there are essentially no atoms with a velocity large enough to Doppler shift them onto one-photon resonance with that beam. However, some velocity class v_R exists such that the two-photon $a \rightarrow c$ transition is resonant. If we then ask what ω_4 must be to be resonant with that same velocity class we are lead to the two equations, $0 = \Delta_{ca} + \vec{k}_{2\gamma} \cdot \vec{v}_R$, and $0 = \Delta_{da} + \vec{k}_4 \cdot \vec{v}_R$. Here $\vec{k}_{2\gamma} = \vec{k}_1 + \vec{k}_2$. We can eliminate v_r and are left with an equation for the 4WM resonance peak position in the $(\Delta_{ca}, \Delta_{da})$ plane,

$$\Delta_{da} = \frac{|\vec{k}_4|}{|\vec{k}_{2\gamma}|}\Delta_{ca}. \tag{9}$$

For the Rb level structure we use, the slope is $\mathcal{M} = k_4/k_{2\gamma} = 0.637$. We measure the slope of the 4WM feature with two calibrated Fabry-Pérot scans for several different detunings of the 795 nm laser, all of which are outside of the single-photon Doppler peak. Figure 7 shows a typical measured resonance structure with the best fit line through the maxima. The result is $\mathcal{M}_{\mathrm{measured}} = 0.62 \pm 0.02$, which is in agreement with the theory.

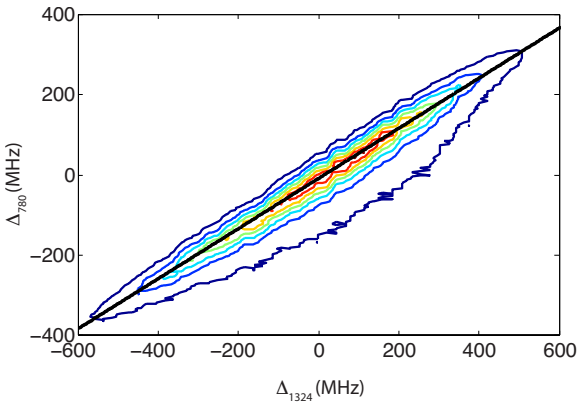

FIG. 7. (Color online) A contour plot of the measured intensity of the 4WM as a function of 1324 and 780 nm laser frequency. The straight line shows a best fit line through the maxima of the resonance feature. The slope agrees well with the theoretical prediction.

C. Conversion efficiency

We define the conversion efficiency of the 4WM process as $\mathcal{E} = I_3(L_{\mathrm{cell}})/I_4(0)$. This is the ratio of the generated 1367 nm light to the 780 nm pump. The efficiencies measured in the experiment are presented in Table I. One could solve the MB equations with parameters similar to that in the experiment, namely, a cell of length $L = 1.5$ cm at temperature $T = 90$ °C and pump powers $P_{795} = 15$ mW and $P_{1324} = 5$ mW. However, the answer is highly dependent on the choice of dipole moments. Since the model we are solving is only a four-level approximation (ignoring the hyperfine and Zee-

TABLE I. Measured experimental 4WM generation efficiencies with $P_{1324} = 5$ mW.

795 nm power (mW)	Efficiency
115	13×10^{-5}
50	4.5×10^{-5}
15	2.4×10^{-5}

man sublevel structure), we cannot expect it to give an accurate estimate of the efficiency. A full Doppler-broadened MB calculation that includes all the relevant atomic levels is a computationally intensive task. Instead we apply perturbation theory and calculate the lowest-order response functions for both fields 3 and 4. We make the approximation that the pump fields 1 and 2 are constant. We assume linear absorption or dispersion to be the dominant process for field 4. Given these assumptions, we may solve the wave equation for E_4 and get

$$E_4(z) = E_4(0)e^{\alpha\bar{\chi}_1 z}. \tag{10}$$

Here $\alpha = 2\pi k_4 \tilde{\mu}_{da}^2 N/\hbar$ and $\bar{\chi}_1$ is the Doppler averaged linear-response function which includes all relevant structure of the $5P_{3/2}$ excited and $F=3 5S_{1/2}$ ground states (see the Appendix). Here $\tilde{\mu}_{da} = \langle \alpha' L' \| r \| \alpha L \rangle$ is the reduced dipole matrix element. All the six-J and three-J symbols have been absorbed into the definition of χ_1. We consider only phase-matched emission into field 3 and insert the result into the wave equation, yielding

$$\partial_z E_3 = \kappa \bar{\chi}_3 E_4^*, \tag{11}$$

where $\kappa = 2\pi k_3 \tilde{\mu}_{dc}\tilde{\mu}_{ad}\tilde{\mu}_{ba}\tilde{\mu}_{cb} N E_1 E_2/\hbar^3$ and $\bar{\chi}_3$ is the Doppler-broadened nonlinear susceptibility which takes all relevant atomic structure into account (see the Appendix). Again the tilde denotes reduced dipole moments. The numerical values for these are $\tilde{\mu}_{ba} = \tilde{\mu}_{da} \approx 5.2 e a_o$ and $\tilde{\mu}_{cb} = \tilde{\mu}_{cd} \approx 5.2 e a_o$. We solve this simple differential equation subject to the boundary condition $E_3(0) = 0$ and get

$$E_3(z) = \frac{\kappa \bar{\chi}_3}{\alpha \bar{\chi}_1^*} E_4(0)(e^{\alpha \bar{\chi}_1^* z} - 1). \tag{12}$$

In the limit that the interaction region (the cell) is much longer than the characteristic absorption length of field 4, we can take $z \to \infty$. The exponential in Eq. (12) then goes to zero and the efficiency becomes

$$\mathcal{E} = \left(\frac{\kappa}{\alpha}\right)^2 \left|\frac{\bar{\chi}_3}{\bar{\chi}_1}\right|^2 = \left(\frac{k_3}{k_4}\frac{\mu_{dc}\mu_{ba}\mu_{cb}}{\hbar^2 \mu_{da}} E_1 E_2\right)^2 \left|\frac{\bar{\chi}_3}{\bar{\chi}_1}\right|^2. \tag{13}$$

Notice that the atomic density, N, is absent. To apply Eq. (13) to a Doppler free medium such as an ensemble of cold atoms, one could drop the bars on the response functions, giving a closed-form solution. We have checked that the MB result agrees with Eq. (13) when we restrict the perturbative treatment to the simple 4-level atomic structure.

We do not know of a simple form for the inhomogeneously broadened response functions so we numerically integrate them. For parameters similar to those in the experiment we see a peak theoretical efficiency of 2×10^{-5}. This theoretical efficiency is of the same order as the experimental efficiency, which is reasonable, given the number of approximations we are making (e.g., perturbative response functions, linear absorption, undepleted pumps, plane-wave fields). Clearly, the conversion efficiency of 780 nm light to 1367 nm light is limited by the linear absorption of the medium. One may consider using electromagnetically induced transparency (EIT) to possibly increase the 4WM efficiency [13].

IV. CONCLUSION

We have observed 4WM in the diamond configuration in a warm atomic ensemble of rubidium. We have observed narrow features in the 4WM gain that arise from velocity-class selective resonant enhancement. We have measured the efficiency of the 4WM process and have shown it to be low, on the order of 1×10^{-4} due to the linear absorption of the pump beam.

ACKNOWLEDGMENT

This work was supported by NSF, DURIP, and CONACYT.

APPENDIX: CALCULATION OF THE SUSCEPTIBILITIES

We present in this appendix how we calculate the susceptibilities, χ_1 and χ_3, used in Eqs. (10)–(13). To calculate χ_1 we use the fact that the 780 nm laser, or field 4, is resonant with the $5S_{1/2}$ $F=3$ ground state to the $5P_{3/2}$ $F=4$ excited state and ignore the other $F=2$ ground-state manifold. Atoms that are Doppler shifted into resonance with the $5P_{3/2}$ $F=3$ and $F=2$ states contribute to the absorption, so we keep those states as well. We assume linearly polarized light along the $\hat{x}$ direction and all field propagation along $\hat{z}$. Summing over all allowed transitions between magnetic sublevels and averaging over the initial states gives us

$$\chi_1 = \frac{i}{12}\left(\frac{1}{\delta_4} + \frac{35}{81}\frac{1}{\delta_3} + \frac{10}{81}\frac{1}{\delta_2}\right). \tag{A1}$$

Here $\delta_j = \Delta_{d_j a_3} - i\Gamma_{d_j a_3}$. The state labels (e.g., d_4) refer to hyperfine states indicted in Fig. 1 and the subscripts indicate the F sublevel.

We again only consider the $F=3$ portion of the ground-state manifold for the calculation of χ_3. Because the 795 laser is far detuned from the $5P_{3/2}$ states we must keep both the contribution from the $F=2$ and $F=3$ hyperfine states. In the experiment the 795 and 1324 nm lasers are tuned to two-photon resonance to the $6S_{1/2}$ $F=3$ manifold. We ignore the $F=2$ upper state. From Fig. 4 it is clear that the 4WM process is strongest through the $5P_{3/2}$ $F=4$ states so we keep only terms involving that state and disregard the contributions from the rest of the D_2 line. Fields 1 and 2 are taken to be polarized in the $\hat{y}$ direction while field 4 is polarized along $\hat{x}$. This choice of polarization forces the generated field 3 to be polarized along $\hat{x}$ as well. The result is

$$\chi_3 = \frac{i}{12}\frac{1}{18}\frac{1}{(\Delta_{d_4 a_3} + i\Gamma_{d_4 a_3})(\Delta_{c_3 a_3} - i\Gamma_{c_3 a_3})} \times \left[\frac{1}{(\Delta_{b_3 a_3} - i\Gamma_{b_3 a_3})} + \frac{1}{(\Delta_{b_2 a_3} - i\Gamma_{b_2 a_3})}\right]. \tag{A2}$$

We arrive at the Doppler-broadened response functions following the prescription of Eq. (5).

[1] R. W. Boyd, M. S. Malcuit, D. J. Gauthier, and K. Rzazewski, Phys. Rev. A **35**, 1648 (1987).
[2] R. E. Slusher, L. W. Hollberg, B. Yurke, J. C. Mertz, and J. F. Valley, Phys. Rev. Lett. **55**, 2409 (1985).
[3] V. Boyer, A. M. Marino, and P. D. Lett, Phys. Rev. Lett. **100**, 143601 (2008).
[4] V. Boyer, A. M. Marino, R. C. Pooser, and P. D. Lett, Science **321**, 544 (2008).
[5] M. Eisaman, A. Andre, F. Massou, M. Fleichhauer, A. Zibrov, and M. Lukin, Nature (London) **438**, 837 (2005).
[6] D. N. Matsukevich, T. Chaneliere, M. Bhattacharya, S. Y. Lan, S. D. Jenkins, T. A. B. Kennedy, and A. Kuzmich, Phys. Rev. Lett. **95**, 040405 (2005).
[7] G. Morigi, S. Franke-Arnold, and G.-L. Oppo, Phys. Rev. A **66**, 053409 (2002).
[8] T. Chaneliere, D. N. Matsukevich, S. D. Jenkins, T. A. B. Kennedy, M. S. Chapman, and A. Kuzmich, Phys. Rev. Lett. **96**, 093604 (2006).
[9] R. T. Willis, F. E. Becerra, L. A. Orozco, and S. L. Rolston, *Laser Science XXIV*, in OSA Technical Digest (CD) (Optical Society of America, Washington DC, 2008), p. 137.
[10] F. E. Becerra, R. T. Willis, S. L. Rolston, and L. A. Orozco, Phys. Rev. A **78**, 013834 (2008).
[11] W. Z. Zhao, J. E. Simsarian, L. A. Orozco, and G. D. Sprouse, Rev. Sci. Instrum. **69**, 3737 (1998).
[12] R. W. Boyd, *Nonlinear Optics* (Academic, New York, 2003).
[13] L. Deng, M. Kozuma, E. W. Hagley, and M. G. Payne, Phys. Rev. Lett. **88**, 143902 (2002).